Temporal analysis of active and passive transport in living cells

Arcizet, D.; Meier, B.; Sackmann, E.; Rädler, J.O.; Heinrich, D.M.

Temporal Analysis of Active and Passive Transport in Living Cells

Delphine Arcizet,[1,2,*] Börn Meier,[1] Erich Sackmann,[3] Joachim O. Rädler,[1] and Doris Heinrich[1]

[1]*Center for NanoScience (CeNS) and Faculty of Physics, Ludwig-Maximilians Universität, Geschwister-Scholl-Platz 1, D-80539 Munich, Germany*

[2]*Laboratoire Matière et Systèmes Complexes, UMR 7057 CNRS & Université Paris Diderot, F-75205 Paris Cedex 13, France*

[3]*Physik Department E22, Technische Universität Munich, D-85748 Garching, Germany*

(Received 23 May 2008; published 12 December 2008)

The cellular cytoskeleton is a fascinating active network, in which Brownian motion is intercepted by distinct phases of active transport. We present a time-resolved statistical analysis dissecting phases of directed motion out of otherwise diffusive motion of tracer particles in living cells. The distribution of active lifetimes is found to decay exponentially with a characteristic time $\bar{\tau}_A = 0.65$ s. The velocity distribution of active events exhibits several peaks, in agreement with a discrete number of motor proteins acting collectively.

DOI: 10.1103/PhysRevLett.101.248103 PACS numbers: 87.16.Uv, 83.10.Pp, 87.16.Ln, 87.16.Wd

Living matter exhibits exceptional dynamical properties, caused by the presence of ATP-driven motion. In particular, the intracellular transport of cargos proceeds by an intricate stochastic interplay between diffusion and active movement along microtubules by means of kinesin and dynein motor proteins [1,2]. The presence of several motor types interacting with cytoskeleton filaments and their balance of binding affinities is pivotal to many physiological processes such as axonal transport in neurons [3] or targeted vesicle transport in eukaryotic cells [4,5]. Dysfunction of the motor mechanical activity has been identified as a key factor in several lethal neurodegenerative diseases [6]. While passive Brownian motion allows intracellular transport of small molecules, it becomes inefficient for large proteins, vesicles and organelles on the scale of a whole cell. Hence the three-dimensional transport of vesicles is supported by motor proteins that move along cytoskeleton filaments, allowing fast physiological responses to external stimuli [7]. Recent theoretical works indeed show that a superposition of free diffusion and phases of active transport that occur randomly and iteratively on a subsecond time scale, results in enhanced reaction kinetics [8,9].

In experimental studies, tracking of single particles is increasingly used for passive *in situ* microrheology [10,11]. The mean square displacement (MSD) functions exhibit distinct regimes on different time scales. Short time scales are dominated by thermal diffusion, while the footprint of active motion appears at longer time scales ($t >$ 1 s). However, such approaches reach their limit when typical residence times within a network mesh and typical transport times along filaments are of the same order of magnitude. A temporal analysis of single particle transport has been carried out on trajectories of labeled vesicles [12,13] or viruses [14] in single cells, revealing successive phases of diffusion and active transport. However, in most of these studies, path dissection is performed manually. Apart from the subjectiveness of using visible criteria, these approaches are very time-consuming. Therefore, an automated and reliable time-resolved identification of motility state signatures is experimentally challenging and of fundamental interest for our understanding of biological transport processes.

In this Letter, we investigate the motion of micron-sized beads in the amoeba Dictyostelium Discoideum (DD). DD is a suitable model cell because of its cytoskeleton simplicity. Unlike most eukaryotic cells, it has no intermediate filaments, nor actin stress fibers. It exhibits a thin actin cortex close to the membrane and is mainly interspersed with asterlike microtubules ranging from the centrosome to the cortex, where they are anchored [15]. In addition, the cytoplasm is highly crowded, consisting of organelles, fixed compartments and freely moving vesicles. Microbeads are readily phagocytosed by DD cells and remain trapped in endosomes [16], thus resembling endogenous vesicles. They can bind to and be dragged along microtubules by dynein and kinesin motors. Here we present a rolling-average algorithm able to reliably separate the active and passive motion of particles in cells. Our approach is based on the analysis of the tracer MSD and directional persistence. We analyze the particle motion in terms of a two-state motility model: this yields the distribution of active and passive state durations as well as the distribution of the state parameters, i.e., the velocity during active phases and the diffusion coefficient of the passive motion. The velocity distribution of active events shows a sequence of equally spaced peaks, revealing the signature of a finite number of molecular motors working collectively. In contrast, after depolymerization of microtubules, the analyzed paths exhibit no significant active event, proving that active states are due to tracer transport along the microtubules exclusively.

Experiments were performed using 1.4 μm ferromagnetic beads as tracer particles, internalized by DD amoebas

in the vegetative state, when they exhibit a quasispherical shape and no aggregation behavior [16]. Bright-field imaging was performed using an Axiovert 200 microscope (Zeiss, Germany) and a CCD camera (C 4880-80 Hamamatsu, Germany). The tracer positions were tracked by a homemade real-time image processing software [17]. Microfluidic stop-flow experiments were carried out using 1 μm latex beads suspended in water, inside a μ-Slide chamber (Ibidi,Germany). The beads were actively moved with a suction control pressure pump (Nanion, Germany). Pressure steps of equal amplitude and duration ($T_0 = 3$ s) with random time intervals (from 5 to 30 s) were assigned numerically (Labview, NI, USA), as depicted in Fig. 1.

Time-resolved MSD analysis is performed as follows: for each time point t of the particle path, the local MSD function over M frames [corresponding to a time window T cf. Fig. 1(a)] is calculated according to:

$$\Delta R_t^2(\delta t) = \langle (\mathbf{R}(t' + \delta t) - \mathbf{R}(t'))^2 \rangle_{-(T/2)<t'<(T/2)} \quad (1)$$

and fitted by a power law $\Delta R_t^2(\delta t) = A\delta t^{\alpha}$. α carries information about the local motion type: for $\alpha = 1$, the particle undergoes Brownian-type diffusion, while for $\alpha = 2$ it is actively transported. The directional persistence of the bead motion is measured in an analogous way, by the standard deviation of the angle correlation function:

$$\Delta\phi_t(\delta t) = \langle (\phi(t' + \delta t) - \phi(t'))^2 \rangle^{1/2}_{-(T/2)<t'<(T/2)}, \quad (2)$$

which is equal to zero for a unidirectional motion. We use here $\Delta\phi(\delta t = T/4)$, with $T/4$, smaller than the total rolling window T, chosen to take into account microtubule bending during a motor-driven event. We name a state

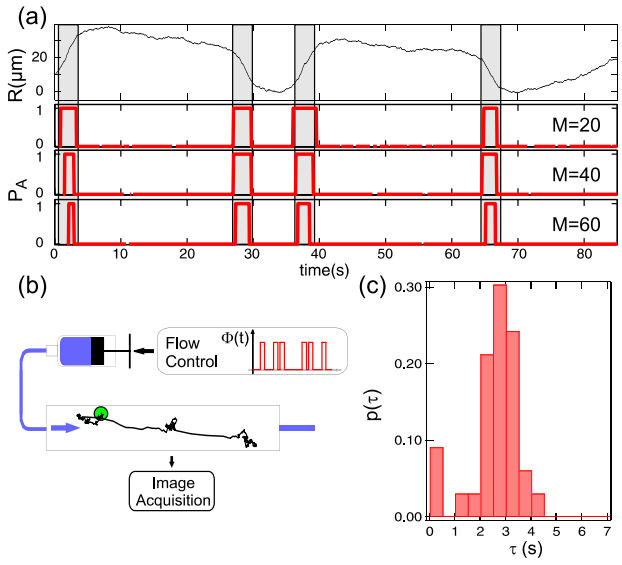

FIG. 1 (color online). Microfluidic test experiment: (a) bead displacement analysis during a stop-flow random sequence: $R(t)$ (top), and $p_A(t)$ for increasing window sizes (bottom), with applied steps shown in light gray; (b) scheme of the microfluidic setup; (c) PDF of active state durations, as extracted from the test sequence of equally long events ($M = 40$).

"active" if both criteria are fulfilled: α close to 2 and $\Delta\phi$ close to 0. We define a binary state variable p_A:

$$p_A = \begin{cases} 1 & \text{if } \alpha = 2 \pm \sigma_\alpha \wedge \Delta\phi = 0 \pm \sigma_\phi \\ 0 & \text{otherwise} \end{cases} \quad (3)$$

$p_A = 1$ indicates an active state (A state), $p_A = 0$ a passive state (P state). During each A state (respectively, P state), we retrieve the local velocity $V = \sqrt{A}$ (respectively, diffusion coefficient $D = A/4$) and the total state duration τ_A respectively, τ_P). We set $\sigma_\alpha = 0.3$ and $\sigma_\phi = 0.6$ in order to achieve sufficient discrimination of motility states.

In order to validate the trajectory analysis, microfluidic test experiments were performed as shown in Fig. 1. The algorithm precisely extracts the A states [see Fig. 1(a) with $M = 40$]. The probability distribution function (PDF) of active state durations is peaked at the predicted value $T_0 = 3$ s [Fig. 1(c)]. The algorithm performance is tested by varying the ratio between step duration T_0 and window size T. Choosing the optimal window size is a trade-off between resolution and accuracy. For the following experiments on living cells, the time window was chosen as 200 ms, leading to a minimum time resolution for the extraction of A states of the same order. Above this threshold, the accuracy in the evaluation of A state durations is estimated as $\sim$100 ms (half a window size).

Figures 2(a) and 2(b) show an example of bead path inside a living DD cell, and demonstrate the outcome of the algorithm, based on both the local MSD exponent value and path persistence. From the frame superimposed on the data in Fig. 2(b), the local MSD curves retrieved at each time point are shown in Fig. 2(c). They exhibit clear power-law behaviors, with exponents clustered around 1 or 2. The sequence in this frame shows a transition from a diffusive state (blue curve) to an active state (red curve, shaded window): the coincidence of α approaching 2 and $\Delta\phi$ falling to zero assigns our state variable for active motion p_A to 1. It should be noted that we do find exponents close to 2 during the A states, higher than the maximal value of 3/2 usually observed in cells [5]. This indicates that by looking at small enough time scales, we have access to the actual transport phases, that are responsible for the enhanced diffusion observed on longer time scales. Also, the MSD exponent during P states is close to 1 [Fig. 2(c)], significantly larger than non integer exponents of 3/4 or smaller reported on other cell types [5,18], where the cytoskeleton viscoelasticity, due to the cross linked and bundled actin network, is important.

The binary dissection of the bead tracks leads to interesting findings: first, the probability distribution of the velocity V retrieved during the A states is narrower than the log-normal PDF of the instantaneous velocity V_{inst} before extraction of the active motions [Fig. 3(a)]. The mean velocity of A states $\bar{V}_A = 0.39\ \mu\text{m s}^{-1}$ is in good agreement with values reported for cargo displacements along microtubules [19]. This indicates that we are able to isolate single active transport tracks of the tracer bead

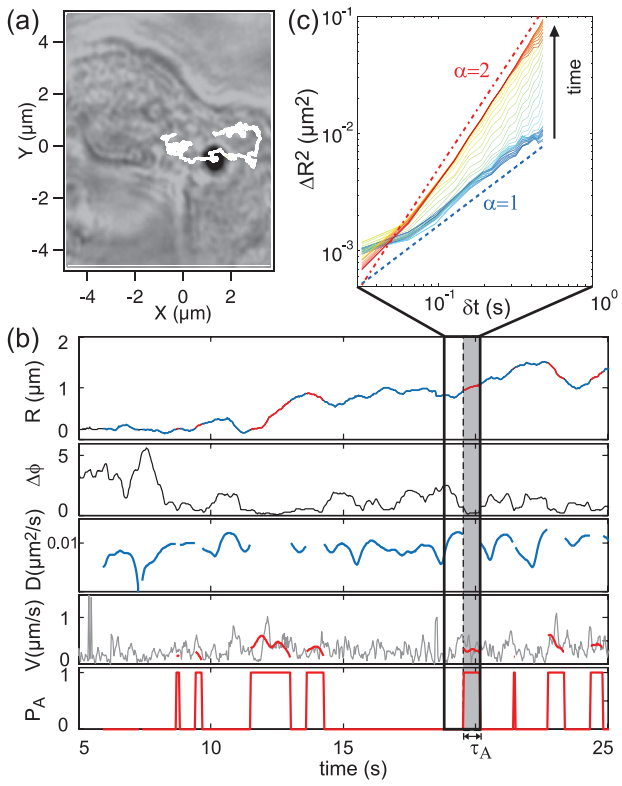

FIG. 2 (color). Living DD cell experiment: (a) transmission image, with the internalized bead 2D path superimposed in white. (b) Bead motion characteristics, from the top to the bottom: displacement $R(t)$ with passive (blue) and active (red) states, standard deviation $\Delta\phi$ of the angle correlation function, diffusion coefficient $D(t)$ retrieved during the P states, instantaneous velocity (light gray) and algorithm-retrieved velocity during the A states (red), and active motion probability p_A. The shaded part of the frame highlights an A state, of duration τ_A. (c) Examples of power-law fits on local MSD functions (thin lines, color-coded for time), with trends for $\alpha = 1$ (blue dashed line) and 2 (red dash-dotted line).

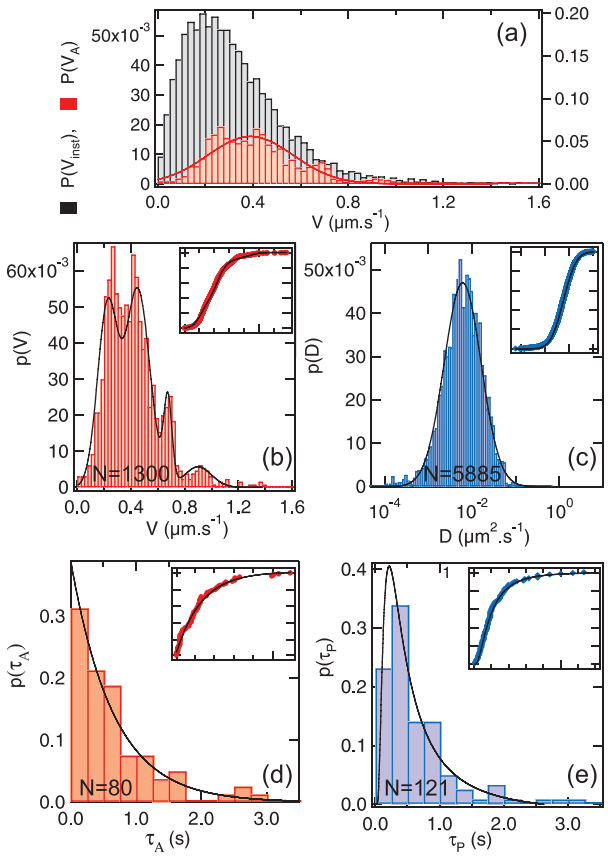

FIG. 3 (color). Analysis of active and passive noise spectra in a living DD cell: PDF of (a) velocity of all events V_{inst} (gray) and of A states V_A (red), (b) A state velocity (superposition of 5 Gaussians, of means $v_n = nv_1$, $v_1 = 0.225\ \mu\text{m}\cdot\text{s}^{-1}$, $n = 1$ to 5), (c) P state diffusion coefficient D (log-normal fit of median $\bar{D} = 6.1 \times 10^{-3}\ \mu\text{m}^2\,\text{s}^{-1}$), (d) A state durations τ_A (exponential decay fit with $\bar{\tau}_B = 0.65$ s), and (e) P state durations τ_P (log-normal fit of median $\bar{\tau}_P = 0.45$ s). N is the number of data points per histogram. Fits are performed on the cumulative probabilities, shown in insets.

along microtubules, which is verified by fluorescent images of the microtubule network during the bead experiments (data not shown). A closer look at the velocity distribution [Fig. 3(b)] reveals several regularly spaced peaks at $v_n \simeq nv_1$ (with $v_1 = 0.225\ \mu\text{m}\,\text{s}^{-1}$). The fact that we observe discrete maxima could indicate that the action of a small number of motors, either dynein or kinesin, collectively dragging the bead, is detected. Several maxima in the velocity distribution have already been observed experimentally for small labeled vesicles carried along microtubules [2], but had never been reported in bead microrheology experiments. Recent models predict them within the so-called "tug-of-war" mechanism, as a signature of the counteracting or cooperative action of molecular motors [20]. The peaks in the active velocity distribution are expected to be regularly spaced for cargos with a high friction coefficient [4], which is likely to correspond to the situation here, considering the bead size. In order to further prove that the active events are related to microtubule-assisted motor proteins, we treated cells with 10 μM Benomyl, a drug known to cause microtubule depolymerization [21]. As shown in Fig. 4, only two very short events of active transport are found after this drug treatment ($\tau_A < 100$ ms).

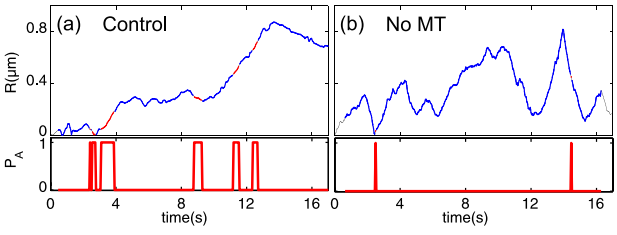

FIG. 4 (color online). Bead motion analysis: $R(t)$ (top) and $P_A(t)$ (bottom), (a) in a normal cell and (b) in a cell whose microtubule network is disrupted by Benomyl: almost no active transport event is found in this case.

Second, the PDF of the purely passive diffusion coefficient is in good agreement with a log-normal law [Fig. 3(c)], indicating that a wide range of phenomena is still included in these P states, probably due to the heterogeneity of the DD cytoplasm. The median value $\bar{D} = 6.1 \times 10^{-3}\ \mu\mathrm{m}^2\,\mathrm{s}^{-1}$ yields an estimate of the cytoplasm viscosity $\eta_c = \frac{k_B T}{6\pi R \bar{D}} \simeq 5 \times 10^{-2}$ Pa s, significantly lower than values retrieved by active microrheology measurements in amoebas (one to 3 orders of magnitude, see [22,23]). Active microrheology mainly probes the stiffest response of the system, namely, the periods during which the tracer is anchored to cytoskeleton filaments, while here, only the Brownian contribution of the bead motion inside the cytoplasm is taken into account. Hence, our $\bar{D}$ is comparable to the values obtained by passive microrheology, even on other cell types [24].

Combining the cytoplasmic friction measured during the P states and the velocity of the first maximum in the V_A distribution, we retrieve a force of $F = 6\pi\eta_c R v_1 \simeq 0.15$ pN, consistent with typical forces developed in cells by a single motor such as kinesin or dynein [25]. Our algorithm further extracts the temporal spectrum of motor activity inside living cells [Fig. 3(d)]: the τ_A distribution exhibits an exponential decrease of characteristic time $\bar{\tau}_A = 0.65$ s. This is expected for a first-order unbinding kinetics of motors walking along filaments [26]. In good agreement with our results, the model of Loverdo *et al.* predicts a maximal enhancement of reactivity in active media for an estimated mean duration of order 0.1 s [9].

The P state duration PDF exhibits a different behavior, clearly distinguishable from a single exponential tail. We fit it by a log-normal law [Fig. 3(e)], as it certainly reflects the superposition of processes occurring on various time scales: free diffusion of the bead in the viscous cytoplasm, mechanical blocking and transient stopping by filaments and organelles, binding time of motors to microtubules (see comments made by Huet *et al.* [13]). The variety of these processes is not investigated here.

In conclusion we have shown that the motion of endocytosed beads in DD can be described by a two-state motion model. Our rolling MSD algorithm robustly retrieved active motor-driven processes from a background of diffusive processes, with high temporal resolution. The dissection into distinct motility states reveals the temporal spectrum of motor protein activity on the one hand, as well as an improved, unbiased assessment of diffusion and hence the cytoplasm viscosity on the other hand. The activity spectrum, combined with specifically labeled vesicles or functionalized particles, could serve as a real-time sensitive indicator of cell response to drug treatment. The time-resolved measurement of the stochastic events might prove of interest to identify molecular interactions that play a role in targeted vesicle transport, enabling a direct comparison to existing models. In general, this algorithm can be used to analyze any two-state trajectories, such as the hunting for preys by animals [27].

The authors acknowledge S. Youssef for computational advice, E. Frey and T. Franosch for helpful discussions and G. Gerisch for providing the cells. This work was supported by the Ecole Normale Supérieure (Paris, France) and by the Excellence Cluster *NIM* (Nanosystems Initiative Munich, Germany).

*delphine.arcizet@physik.lmu.de

[1] S. Rice *et al.*, Nature (London) **402**, 778 (1999).
[2] C. Kural *et al.*, Science **308**, 1469 (2005).
[3] L. Goldstein and Z. Yang, Annu. Rev. Neurosci. **23**, 39 (2000).
[4] S. Klumpp and R. Lipowsky, Proc. Natl. Acad. Sci. U.S.A. **102**, 17 284 (2005).
[5] A. Caspi, R. Granek, and M. Elbaum, Phys. Rev. E **66**, 011916 (2002).
[6] F. M. Laird *et al.*, J. Neurosci. **28**, 1997 (2008).
[7] C. Bouzigues, M. Morel, A. Triller, and M. Dahan, Proc. Natl. Acad. Sci. U.S.A. **104**, 11 251 (2007).
[8] S. Klumpp and R. Lipowsky, Phys. Rev. Lett. **95**, 268102 (2005).
[9] C. Loverdo *et al.*, Nature Phys. **4**, 134 (2008).
[10] G. Lenormand *et al.*, Biochem. Biophys. Res. Commun. **360**, 797 (2007).
[11] C. Raupach *et al.*, Phys. Rev. E **76**, 011918 (2007).
[12] K. D. Girard, S. C. Kuo, and D. N. Robinson, Proc. Natl. Acad. Sci. U.S.A. **103**, 2103 (2006).
[13] S. Huet *et al.*, Biophys. J. **91**, 3542 (2006).
[14] K. de Bruin *et al.*, Molec. Therapy **15**, 1297 (2007).
[15] S. Ma and R. Chisholm, J. Cell Sci. **115**, 1453 (2002).
[16] D. Heinrich and E. Sackmann, Acta Biomat. **2**, 619 (2006).
[17] J. E. Schilling, E. Sackmann, and A. R. Bausch, Rev. Sci. Instrum. **75**, 2822 (2004).
[18] K. Van Citters *et al.*, Biophys. J. **91**, 3946 (2006).
[19] G. Schuetz *et al.*, Microsc. Res. Tech. **63**, 159 (2004).
[20] M. Müller, S. Klumpp, and R. Lipowsky, Proc. Natl. Acad. Sci. U.S.A. **105**, 4609 (2008).
[21] K. Gupta *et al.*, Biochemistry **43**, 6645 (2004).
[22] W. Feneberg, M. Westphal, and E. Sackmann, Eur. Biophys. J. **30**, 284 (2001).
[23] S. Marion *et al.*, J. Cell Sci. **117**, 3271 (2004).
[24] Y. Tseng, T. Kole, and D. Wirtz, Biophys. J. **83**, 3162 (2002).
[25] R. Mallik *et al.*, Nature (London) **427**, 649 (2004).
[26] E. Frey, A. Parmeggiani, and T. Franosch, Genome Inform. **15**, 46 (2004).
[27] D. L. Kramer and R. L. McLaughlin, American Zoologist **41**, 137 (2001).